molecules

MDPI

Review

Design and Synthesis Strategy of MXenes-Based Anode Materials for Sodium-Ion Batteries and Progress of First-Principles Research

Dan Su [1], Hao Zhang [2], Jiawei Zhang [1] and Yingna Zhao [1,3,*]

[1] Hebei Province Laboratory of Inorganic Nonmetallic Materials, College of Material Science and Engineering, North China University of Science and Technology, Tangshan 063210, China; 15612578603@163.com (D.S.); zhangpepsi007@163.com (J.Z.)
[2] College of Clinical Medicine, North China University of Science and Technology, Tangshan 063210, China; haozhang0823@foxmail.com
[3] Hebei (Tangshan) Ceramic Industry Technology Research Institute, Tangshan 063007, China
* Correspondence: zhyn@ncst.edu.cn; Tel.: +86-138-3155-1024

Abstract: MXenes-based materials are considered to be one of the most promising electrode materials in the field of sodium-ion batteries due to their excellent flexibility, high conductivity and tuneable surface functional groups. However, MXenes often have severe self-agglomeration, low capacity and unsatisfactory durability, which affects their practical value. The design and synthesis of advanced heterostructures with advanced chemical structures and excellent electrochemical performance for sodium-ion batteries have been widely studied and developed in the field of energy storage devices. In this review, the design and synthesis strategies of MXenes-based sodium-ion battery anode materials and the influence of various synthesis strategies on the structure and properties of MXenes-based materials are comprehensively summarized. Then, the first-principles research progress of MXenes-based sodium-ion battery anode materials is summarized, and the relationship between the storage mechanism and structure of sodium-ion batteries and the electrochemical performance is revealed. Finally, the key challenges and future research directions of the current design and synthesis strategies and first principles of these MXenes-based sodium-ion battery anode materials are introduced.

Keywords: MXene; sodium-ion battery; negative electrode materials; density functional theory

check for updates

Citation: Su, D.; Zhang, H.; Zhang, J.; Zhao, Y. Design and Synthesis Strategy of MXenes-Based Anode Materials for Sodium-Ion Batteries and Progress of First-Principles Research. *Molecules* **2023**, *28*, 6292. https://doi.org/10.3390/molecules28176292

Academic Editor: Gregorio F. Ortiz

Received: 24 July 2023
Revised: 16 August 2023
Accepted: 24 August 2023
Published: 28 August 2023

Copyright: © 2023 by the authors. Licensee MDPI, Basel, Switzerland. This article is an open access article distributed under the terms and conditions of the Creative Commons Attribution (CC BY) license (https://creativecommons.org/licenses/by/4.0/).

1. Introduction

In order to cope with the increasingly serious energy crisis and environmental pollution, people are gradually increasing the use of natural resources such as solar, wind and tidal energy; however, due to the complex distribution, discontinuity and other problems, people also need to find energy storage and conversion systems to convert these natural resources into clean energy that can be used by human beings continuously. Secondary batteries are an important class of energy storage devices. Since the commercialisation of lithium-ion batteries in 1991, they have played an important role in mobile electronics, electric vehicles and grid energy storage [1]. However, the high preparation cost, low energy density, and potential safety risks caused by organic electrolytes in lithium-ion batteries (LIBs) have triggered widespread concerns [2]; therefore, there is an urgent need to find alternative battery technologies for low-cost and high-safety applications to meet the stringent requirements of large-scale energy storage devices and a variety of consumer electronics products. Sodium-ion batteries have attracted great interest because they exhibit electrochemical properties similar to those of lithium-ion batteries, and sodium has the advantages of abundant reserves and low cost. However, compared with lithium, sodium has a larger ionic radius (0.102 nm), higher standard reduction potential (−2.71 V vs. standard

hydrogen electrode (SHE)) and lower electronegativity (0.93), which leads to the fact that sodium-ion batteries always suffer from the slow adsorption and insertion of Na+ as well as a large volume expansion [3,4]. This results in sodium-ion batteries with a low reversible capacity and poor cycling stability, which limits the reversible capacity of sodium-ion batteries. The low reversible capacity and poor cycling stability of sodium-ion batteries limit their large-scale generation and use [5–7]. As a result, numerous researchers have focused on developing new sodium storage materials with tuneable chemical structures to improve sodium storage efficiency.

Since the successful exfoliation of graphene in 2004, two-dimensional (2D) materials have attracted great research interest due to their good properties, such as high electrochemical activity [8] and fast ion diffusion pathway [9]. In 2011, an emerging class of 2D materials, MXenes, was successfully prepared, and in the past 10 years, MXenes have been extensively studied, especially in the field of sodium-ion batteries. Extensive and in-depth research has been carried out on MXene materials, especially in the field of sodium-ion batteries. MXenes is a collective name for a class of 2D transition metal carbides or carbonnitrides, whose general formula is denoted as $M_{n+1}X_nT_x$, where M denotes the transition metal element (Ti, Nb, Sc etc.), X is the carbon or nitrogen element and T denotes the terminal surface groups (-O,-F and -OH), which are mainly formed by the use of Hydrofluoric acid or a mixture of hydrochloric acid and lithium fluoride prepared by selective etching of A-layers (Al, Si, and Ga etc.) from the corresponding $M_{n+1}X_nT_x$ phase [10–12]. The highly conductive 2D lamellar structure [13] and tuneable surface chemistry [14] of MXene materials allow them to offer new possibilities as anode materials in solving the problems of slow Na^+ diffusion rate and high diffusion barriers in sodium-ion batteries. However, the collapse and re-stacking of MXene lamellae hinder the full utilisation of MXenes' active sites and limit the large-scale application of MXenes as anodes for sodium-ion batteries. Therefore, numerous researchers have promoted the further practical application of MXene materials in the field of energy storage devices by designing MXenes-based materials that can significantly increase the electronic conductivity and enhance their electrochemical performance while preventing the aggregation of individual nanosheets [15].

Since 2015, MXenes-based materials have developed rapidly in the field of energy storage, and a large number of research articles on sodium-ion batteries have been published. In this review, we first summarise the research work and development in the field of MXenes-based sodium-ion energy storage materials in recent years, focusing on the design and synthesis strategies of MXenes-based sodium-ion battery anode materials currently employed by, and in particular illustrating the effects of, the various design strategies on the structure and properties of MXenes-based materials, as shown in Table 1. On this basis, we also summarise the recent first-principles study of MXenes-based anode materials for sodium-ion batteries to reveal the storage mechanism and the relationship between the structure and electrochemical performance of sodium-ion batteries. Finally, the current challenges and future directions of the design and synthesis strategies and first-principles studies of MXene-based anode materials for sodium-ion batteries are summarised and outlined.

2. Design and Synthesis Strategy of Anode Materials for MXenes-Based Sodium-Ion Batteries

Although MXenes as an emerging anode material for sodium-ion batteries have attracted great research interest, their tendency to aggregate or stack in practical use greatly hinders electron transport, leading to their own low capacity and further limiting the large-scale application of MXenes. In order to solve these problems, researchers have proposed a number of design and synthesis strategies, which we summarise as elemental doping modification, binary material composite and ternary material composite.

2.1. Design and Synthesis of Elementally-Doped MXenes-Based Materials

Elemental doping modification of MXene materials is one of the most common strategies employed by researchers to dope heteroatoms such as nitrogen (N) and sulphur (S)

onto carbon-based materials [16] in order to enhance material specificity. Based on the conventional preparation of sulphur-doped multilayer $Ti_3C_2T_x$ MXene, Bao et al. [17] prepared sulphur-doped $Ti_3C_2T_x$ MXene (S-$Ti_3C_2T_x$) with a 3D folded structure by employing a vacuum freeze-drying method (Figure 1A). The reduction and oxidation peaks of the negative electrodes of the S-$Ti_3C_2T_x$ have a small potential difference between the reduced and oxidised peaks, and the enlarged interlayer spacing of the MXene leads to the electrodes with good dynamic properties. Its initial discharge capacity reached 970 mAh g^{-1}, and the discharge capacity was maintained at 690.3 mAh g^{-1} after 200 cycles with a decay rate of 0.14% per cycle (Figure 1B). The capacity was maintained at 577.1 mAh g^{-1} after 500 cycles at 2C (Figure 1C). Sun et al. [18] produced sulphur-doped Ti_3C_2 MXenes by electrostatic self-assembly (Figure 1D), and the capacity of the electrodes of this material was 135 mAh g^{-1} after 1000 cycles at a current density of 2 A g^{-1}, with an average capacity loss of only 0.033% per cycle. The average capacity loss per cycle was only 0.033%. The heat treatment temperature also has a certain effect on the elemental doping modification, and the S-doped MXene electrode has a larger interlayer spacing and more abundant active sites at high temperature [19]. Li et al. [20] used sulphur as a template to modulate the surface chemistry and microstructure of Ti_3C_2 calcined at 400 °C to obtain the mesoporous thin film of $Ti_3C_2T_x$ (SMX-100), and the results of electrochemical studies showed that the electrode still maintained a stable specific capacity of 206.2 mAh g^{-1} after 200 cycles at 100 mA g^{-1} (Figure 1E), and the SMX-100 electrode consistently maintained a high capacitance during the charge/discharge cycling process (Figure 1F), which was mainly due to the effective penetration of the electrolyte and the increase in the layer spacing caused by the insertion of Na^+. The results show that the incorporation of sulphur terminals can significantly accelerate the redox reactivity of Na–S cells and limit the outward diffusion of polysulfides, so that Na–S cells have higher rate capability.

Nitrogen doping has been shown to be one of the facile modification strategies to improve the electrochemical properties of MXenes [21–23]; however, the position of nitrogen doping has an effect on the electrical properties of MXenes due to the underlying mechanism. Jin et al. [24] synthesised Ti_3C_2 MXenes (SWMP-5) with sandwich structure by using the interfacial self-assembly method to ultrasonicate Ti_3C_2 in poly(vinyl imine) solution (Figure 2A). The dense N-rich polymer with a hydrogen bonding network connects the stable conductive framework to provide a fast channel for Na storage. The SWMP-5 negative electrode has an initial discharge capacity of 338.5 mAh g^{-1} (Figure 2B), and provides excellent multiplicative rates of 224.5, 185, 161, 141, 120, and 105 mAh g^{-1} at current densities ranging from 50–2000 mA g^{-1} capacity (Figure 2C). Fan et al. [25] used poly(melamine) microspheres as templates to treat Ti_3C_2 to obtain N-$Ti_3C_2T_x$ (M8T1) with a highly uniform and well-defined porous framework structure (Figure 2D). The average capacity reaches 180.5 mAh g^{-1} (Figure 2E) at a current density of 25 C (1 C = 200 mA g^{-1}), while the capacity retention after 3500 cycles at a current density of 2 A g^{-1} is 75% (Figure 2F), showing good cycling stability. The sodium-ion storage mechanism demonstrates that the interconnected nanosheets have a porous skeleton structure and high electronic conductivity, forming continuous conductive structures and creating multidimensional ion channels, which is conducive to rapid ion diffusion. The above studies show that surface modification of nitrogen atoms can greatly enhance the electrochemical reactivity and electronic conductivity of materials, and nitrogen doping strategies can induce well-defined porous structure, high surface area and macroporous volume. However, due to the influence of the underlying mechanism, the position of nitrogen doping has a certain influence on the electrical properties of MXenes, and the current research on its position is not comprehensive enough, so further research is still needed.

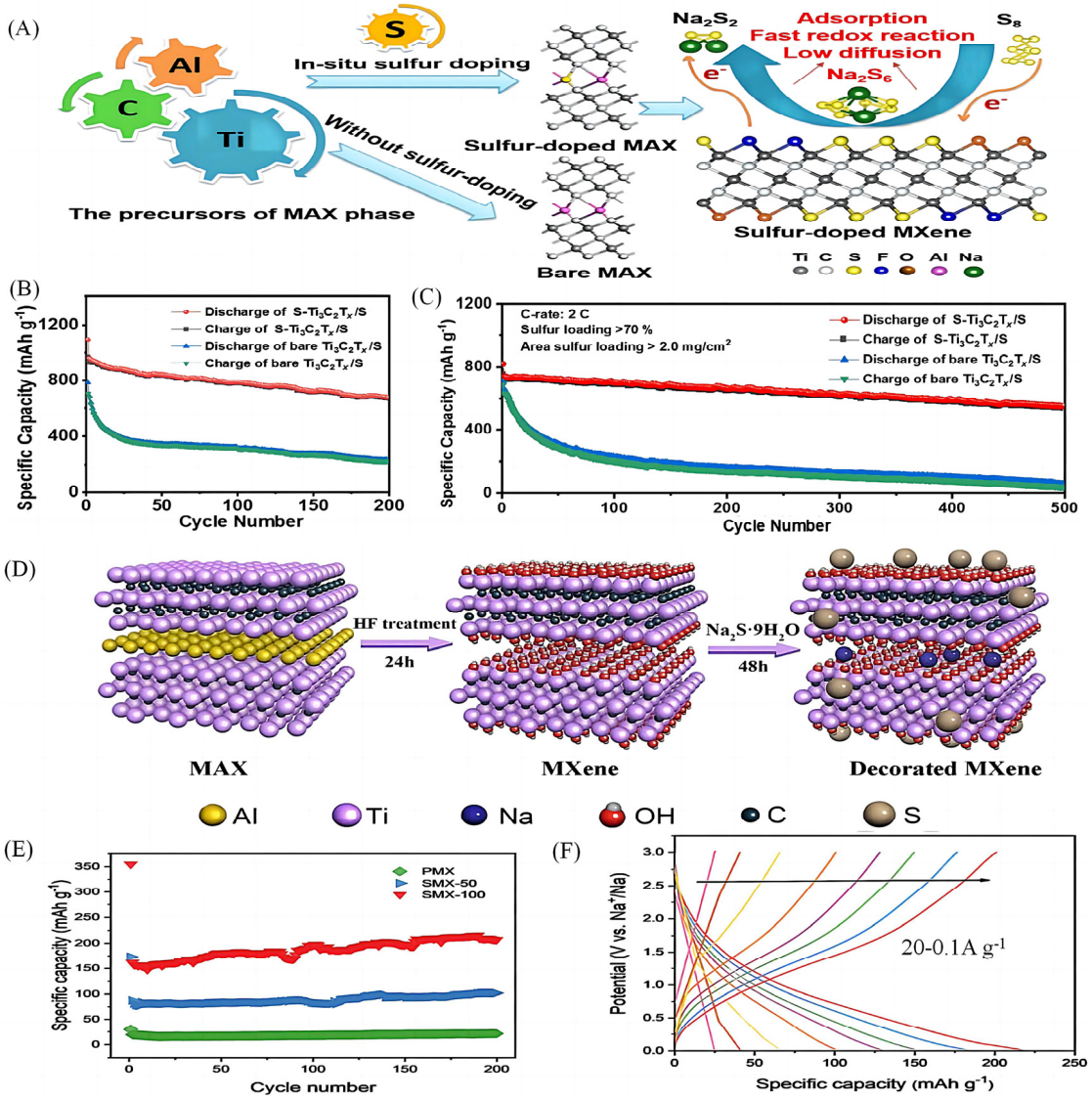


Figure 1. (**A**) Schematic diagram demonstrating the preparation of sulphur-doped MXene [17]. (**B**) Cycling performances of S-$Ti_3C_2T_x$/S electrode and bare $Ti_3C_2T_x$/S electrode at 0.5 C for 200 cycles [17]. (**C**) Cycling performances of S-$T_{i3}C_2T_x$/S cathode and bare $Ti_3C_2T_x$/S cathode at 2 C for 500 cycles [17]. (**D**) Schematic illustration of the preparation of sulphur-decorated Ti_3C_2 MXenes [18]. (**E**) Cycling performances of SMX-100 at 0.1 A g^{-1} [20]. (**F**) Charge–discharge curves at different current densities [20].

2.2. Design of MXenes-Based Binary Composite Synthesis

Compared with elemental doping, the design of- composite systems for MXenes can better solve the problems of slow ion transport due to the large radius of Na^+ and volume expansion during electrochemical sodiation/desodiation [26–28]. Therefore, numerous researchers have focused on the design of MXenes-based binary composites to promote the embedding and de-embedding of Na^+ during the electrochemical process of sodium-ion batteries and to improve the structural durability of the anode of sodium-ion batteries by constructing a binary heterojunction structure, which enhances the relevant performance of sodium-ion batteries. However, different preparation methods will not only affect the interaction between the second phase and MXenes, but also affect the morphology and properties of the composite. In this regard, we summarise the above adopted strategies as hydrothermal or solvent-thermal methods, electrostatic self-assembly methods, in situ synthesis methods and methods such as CVD.

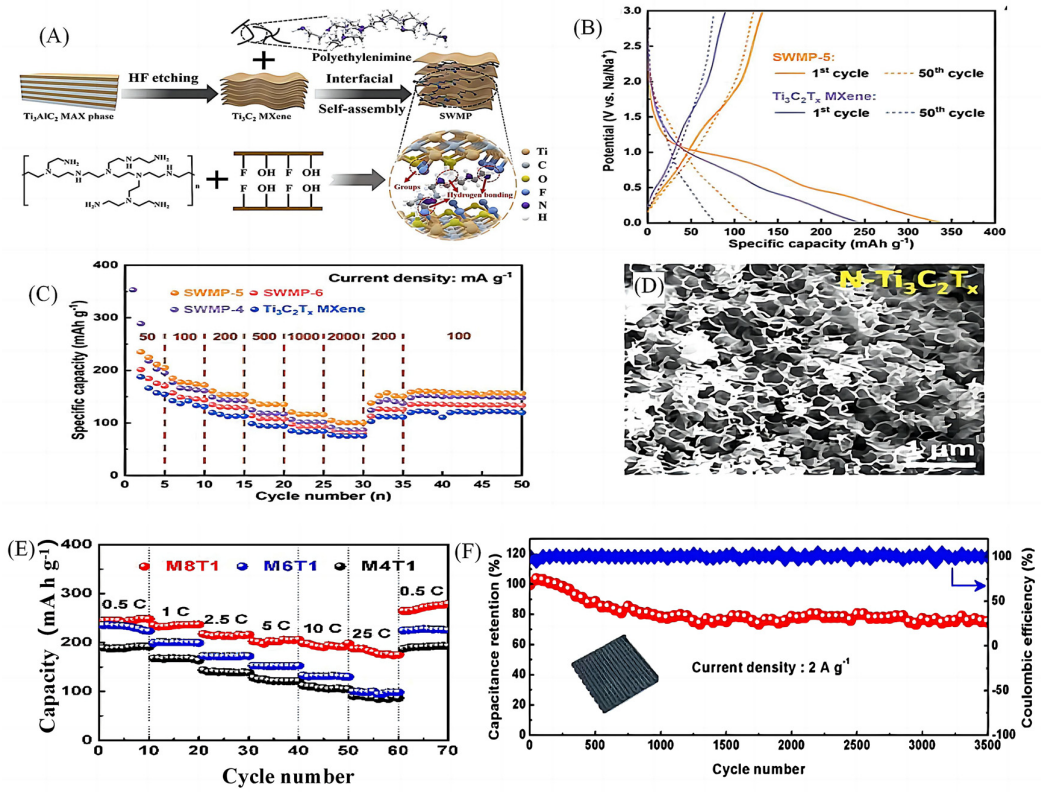


Figure 2. (**A**) Schematic illustration of the interfacial self-assembly MXene-based sandwich-like structure with polymer network [24]. (**B**) The initial and fiftieth cycle of galvanostatic charge/discharge curves of SWMP-5 and $Ti_3C_2T_x$ MXene at 500 mA g^{-1} [24]. (**C**) Rate performance of SWMP-5 [24]. (**D**) SEM images of N-$Ti_3C_2T_x$ (M8T1). (**E**) Rate performances of M8T1[25]. (**F**) Cycling performance of the 3D-printed SIC (SIC-4) at 2 A g^{-1}. Inset: Real photo showing a 3D-printed woodpile N-$Ti_3C_2T_x$ electrode [25].

2.2.1. Hydrothermal Methods

The hydrothermal method is one of the most commonly used methods for the preparation of MXenes-based sodium-ion battery anode materials due to its advantages of easy preparation of nanomaterials with good crystallinity and different shapes and sizes. Wu et al. [29] prepared flower-like three-dimensional VO_2/MXenes sodium-ion battery anode materials in different proportions (Figure 3B) by using the hydrothermal method (Figure 3A) with a 0.1 A g^{-1} current density after 200 cycles with a reversible capacity of 280.9 mAh g^{-1} (Figure 3C). Sun et al. [30] obtained NTO/Ti_3C_2 layered material with a porous structure on the basis of the MXenes' stabilised structure by a two-step hydrothermal method (Figure 3D), and the composite material, after 1900 cycles at a current density of 2000 mA g^{-1}, still provides a reversible capacity of 82 mAh g^{-1} (Figure 3E), which shows excellent stability.

Although the hydrothermal method is simple to operate and can produce a variety of novel and unique morphologies, there are still a series of shortcomings, such as high equipment requirements, long reaction time and high energy consumption. Based on this, more and more researchers are optimizing the hydrothermal method by combining two different preparation methods. Consequently, researchers have improved the hydrothermal method and combined it with other treatments to jointly prepare MXenes-based binary composites with better electrochemical properties, e.g., Xu et al. [31] used a simple hydrothermal method combined with a heat treatment process under H_2 atmosphere to prepare a novel $MoSe_2$/MXenes heterojunction ultrafast kinetic network electrode (Figure 3F). Afterwards, Zhang et al. [32] prepared SnS nanoparticle-modified $Ti_3C_2T_x$ composites using a similar process (Figure 3G). The first-time charge/discharge capacities of SnS/$Ti_3C_2T_x$ were 348.4

and 495.0 mAh g^{-1} (Figure 3I) with a coulombic efficiency of 70.4% (Figure 3H), and at a high current density of 1000 mA g^{-1}. The discharge capacity was still maintained at 255.9 mAh g^{-1}, and the reversible discharge capacity after 50 cycles at a current density of 500 mA g^{-1} was about 320 mAh g^{-1} with a Coulombic efficiency of 98% (Figure 3J). The use of $CoNiO_2$, $CoNi_2O_4$, $NiCo_2O_4$, $CoNi_2S_4$ and other polytransition metal materials with high theoretical capacity and excellent electrical conductivity to enhance the electrochemical performance of MXene materials has also been an area of intense focus in recent years. Tao et al. [33] obtained $CoNiO_2$/MXenes composites through the combination of the hydrothermal method and a heat treatment process, the first-time capacity of the material was 463 mAh g^{-1} and its reversible capacity reached 248.1 mAh g^{-1} in the charging/discharging experiment at 100 mA g^{-1}. The good electrochemical performance of the $CoNiO_2/Ti_3C_2T_x$ composites is attributed to the increase in electrochemically active sites by the nano-$CoNiO_2$ which shortens the diffusion paths of Na^+ during the cycling process. Nevertheless, the long reaction time, complicated operation and high production cost of the hydrothermal method limits its use in large-scale production.

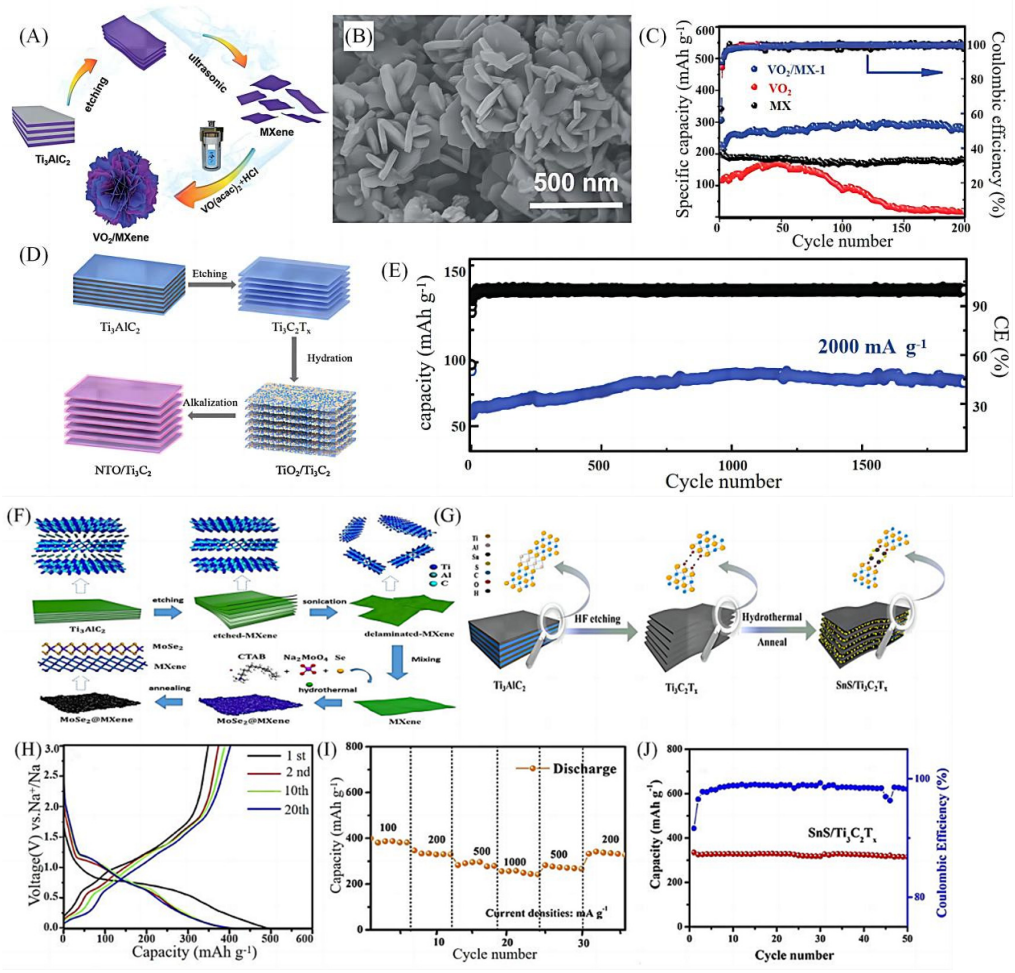


Figure 3. (**A**) Schematic illustration of the synthetic process for VO_2/MXenes hybrids [29]. (**B**) SEM images of the VO_2/MX-1[29]. (**C**) Cyclic performances of VO_2/MX, VO_2 and MX at a current of 0.1 A g^{-1} [29]. (**D**) Schematic illustration for synthesizing the NTO/Ti_3C_2 composite [30]. (**E**) Long-term cycling performance and CE data of the NTO/Ti_3C_2 anode at 2000 mA g^{-1} [30]. (**F**) illustration of the synthesis of single-layer MXenes and $MoSe_2$/MXenes heterojunction [31]. (**G**) The SnS/$Ti_3C_2T_x$ composites were synthesized by hydrothermal and annealing methods [32]. (**H**) The galvanostatic discharge/charge voltage profiles of the SnS/$Ti_3C_2T_x$ composites at 100 mA g^{-1} [32]. (**I**) The rate capability of SnS/$Ti_3C_2T_x$ electrode [32]. (**J**) The cycling performance of SnS/$Ti_3C_2T_x$ composites with a current density of 500 mA g^{-1}, and the corresponding coulombic efficiency [32].

2.2.2. Electrostatic Assembly Method

The self-assembly [34] method of electrochemical modification of the material surface has attracted much attention in the field of energy storage devices due to its simplicity, environmental friendliness, high efficiency, and low cost. Liu et al. [35] assembled VO_2 nanotubes (VO_2-NTs) and $Ti_3C_2T_x$ MXenes into a multidimensional crosslinked structure of VO_2-NTs/Ti_3C_2 anodes via electrostatic assembly. Xie et al. [36] prepared porous $Ti_3C_2T_x$/CNTs composite thin films by electrostatic assembly combined with the chemical vapour deposition (CVD) method, which effectively prevented MXenes from being grafted in the structure. They also used the deposition (CVD) method to prepare porous $Ti_3C_2T_x$/CNTs composite films, in which the grafted carbon nanotube CNTs in the structure effectively prevented the refolding of the MXene nanosheets and formed a porous structure, which facilitated the transport of the electrolyte and the access of ions to the electrodes. Zhao et al. [37] designed a novel molecular level PDDA-BP/Ti_3C_2 nanosheet heterostructure, which effectively discharged for more than 6 h to reach 3.0 V after 60 s of charging using a light-emitting diode (LED). Wu et al. [38], using the unique adsorption behaviours of oxygen-containing functional groups, produced MXenes that were self-assembled with SnS_2 by vacuum-assisted filtration to obtain MXenes/SnS_2 composites with different ratios (Figure 4A,B). The first charge/discharge capacities of the composites (MXenes/SnS_2 = 5:1) at a current density of 100 mA g^{-1} were 460 mAh g^{-1} and 882 mAh g^{-1}, respectively (Figure 4C), and the reversible capacity reached 322 mAh g^{-1} after 200 cycles (Figure 4D). In addition to the common lamellar MXenes-based composites, researchers have also constructed MXenes-based composites with a variety of microscopic morphologies, e.g., Dong et al. [39] used an in situ electrostatic attraction and selenide process to homogeneously anchor $Ni_{0.5}Co_{0.5}Se_2$ nanoparticles to $Ti_3C_2T_x$ conductive structures and prepared structurally stable $Ni_{0.5}Co_{0.5}Se_2/Ti_3C_2T_x$ composites (Figure 4E). Guo et al. [40] also prepared MXenes $Ti_3C_2T_x$ nanosheet-encapsulated titanium oxide sphere structures (TiO_2@$Ti_3C_2T_x$) for the first time by using a self-assembly strategy (Figure 4F), and the MXene layer with high electronic conductivity protects the TiO_2 spheres from electrochemical comminution, forming a stable solid-electrolyte interface. Although the electrostatic self-assembly technology is developing rapidly at present, there are some problems in its theoretical and practical applications, which urgently need to be further solved by researchers.

2.2.3. In Situ Synthesis Method

There are certain problems in the composite materials prepared by the adhesion method, such as the disadvantages of the introduced particle size, unstable thermodynamic properties and low interfacial bonding strength. Such problems can be ameliorated by in situ growth within the matrix through chemical reactions. In recent years, it has become one of the research hotspots to use in situ synthesis technology with the advantages of stable thermodynamic properties, non-polluting interfaces and high bonding strength to prepare MXenes-based binary composite anode materials, which are suitable for the construction of high-performance sodium-ion rechargeable batteries. Tang et al. [41] successfully prepared M-SnP-In composites through the growth of ultra-small SnO_2 nanoparticles (NPs) in the intermediate layer of $Ti_3C_2T_x$ composites (Figure 5A,B), and the M-SnP-In electrode maintained a high capacity of 436.6 mAh g^{-1} after 1500 cycles at a current density of 2A g^{-1} (Figure 5C), which is superior to most sodium-ion batteries reported so far. Ding et al. [42] successfully prepared $FePS_3$@MXenes 2D/2D heterojunction composites by in situ mixing of ultrathin MXene nanosheets with $FePS_3$ nanosheets (Figure 5D,E), and Ming et al. [43] prepared $NaTiO_2$ nanotubes (NTO NTs) on $Ti_3C_2F_x$ in situ as the enhanced sodium-ion battery. The NTO NTs were grown vertically on the $Ti_3C_2F_x$ layer, which promoted Na^+ diffusion and electron transfer and effectively inhibited the aggregation of the $Ti_3C_2F_x$ layer. Zhang et al. [44] proposed a silver-ear-like carbon coated $Ti_3C_2T_x$ (T-MXenes@C) anode material for sodium-ion batteries (Figure 5F,G). Self-polymerisation of dopamine on pristine $Ti_3C_2T_x$ nanosheets effectively promoted the transformation of $Ti_3C_2T_x$ into a silver-ear-like 3D structure, which was then carbonised in inert air to form a thin carbon

coating that would protect the exposed surface of the $Ti_3C_2T_x$ nanosheets from air oxidation and structural aggregation. The 3D silver-ear-like structure with active and stable surface (T-MXene@C) promotes charge transport, improved multiplicity performance and long cycling performance, among others. Despite the advantages of the in situ synthesis method, more in-depth studies on its reaction mechanism, practical applications and process optimisation are still needed to provide new possibilities for its industrial production.

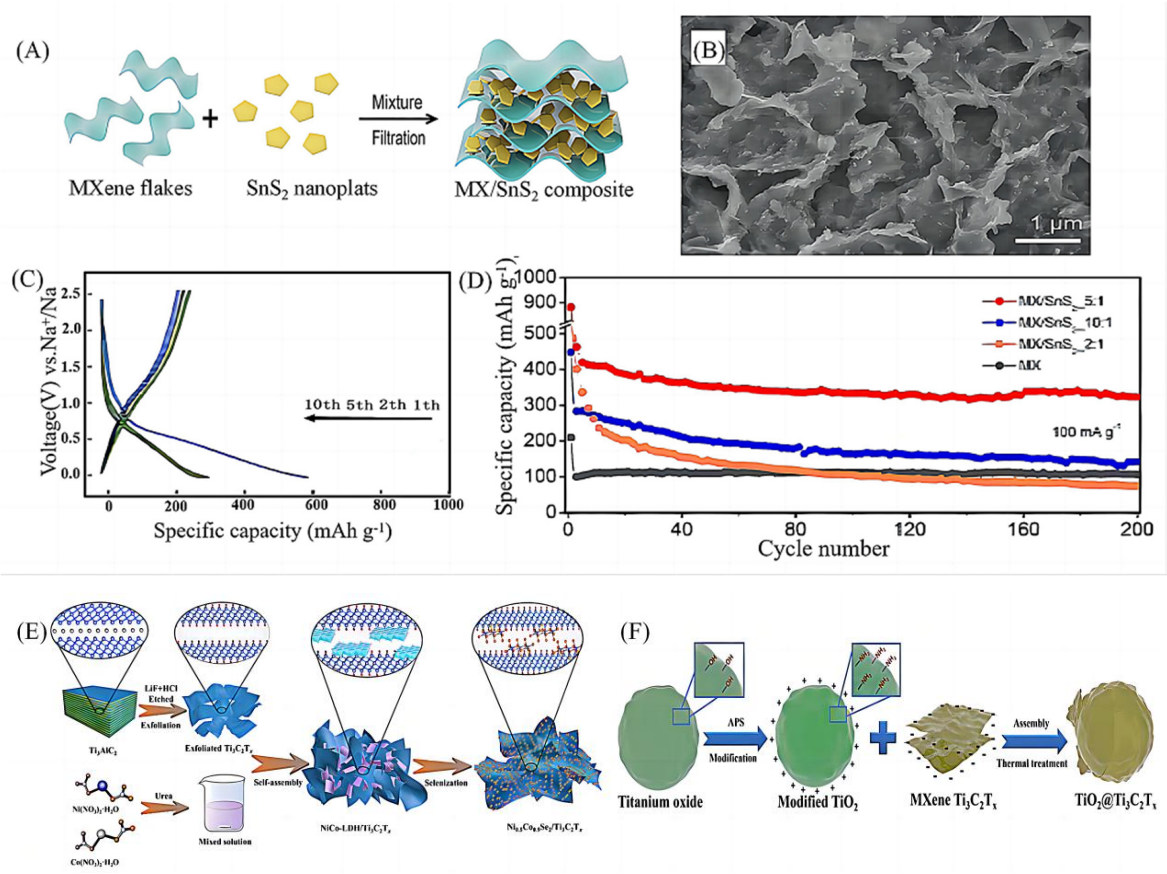


Figure 4. (**A**) The design concept and synthesis process of electrode materials for SIBs with high volumetric and gravimetric capacity [38]. (**B**) SEM images of MX/SnS_2 [38]. (**C**) Galvanostatic charge-discharge profiles of MX/SnS_2 5:1 [38]. (**D**) Rate performance [38]. (**E**) The preparation process of the $Ni_{0.5}Co_{0.5}Se_2/Ti_3C_2T_x$ [39]. (**F**) Schematic illustration of synthetic process for $TiO_2@Ti_3C_2T_x$ material [40].

Although the in situ synthesis method has many advantages, most of the in situ reaction systems are still in the stage of experimentation and development research, and the in situ reaction process is not easy to control, and the formation of intermediate phases cannot be controlled, which adversely affects the properties of materials. The content and ratio of reactants have a great influence on the formation of the reaction and the reaction speed, and it is difficult to control. It is still necessary to carry out more in-depth research on its reaction mechanism, practical application and process optimization to provide new possibilities for its industrial production.

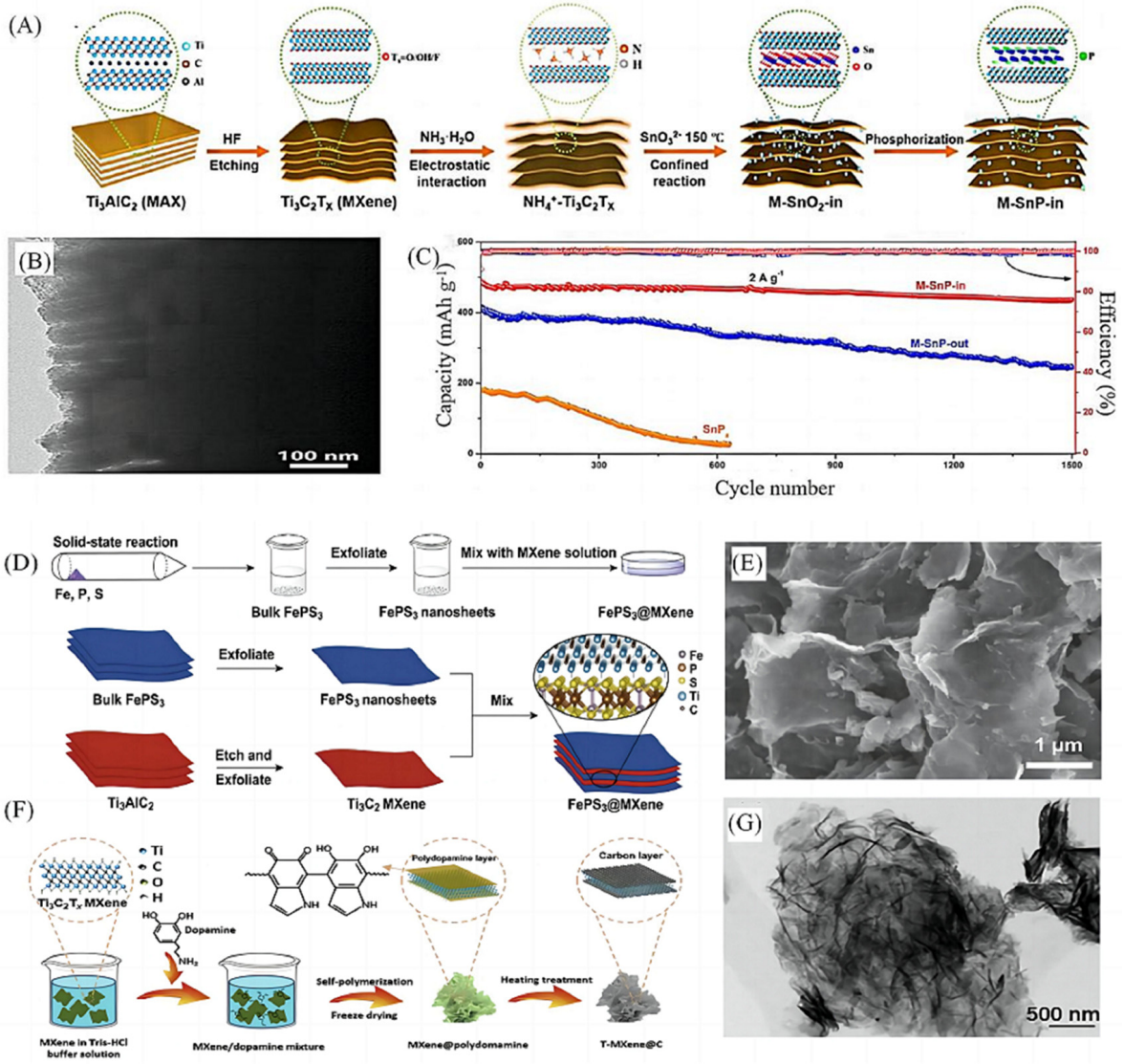


Figure 5. (**A**) Schematic illustration of the strategy for preparing M-SnP-in hybrids [41]. (**B**) Cycling performance tested at 2 A g^{-1} for 1500 cycles [41]. (**C**) Synthesis process diagram of $FePS_3$@MXenes and Schematic illustration of MXenes assembled on $FePS_3$ nanosheets surface and the micromolecular structure in enlarged view $FePS_3$@MXenes [41]. (**D**) SEM images of $FePS_3$@MXenes [42]. (**E**) Schematic diagram generalizing the preparation [42]. (**F**) Schematic diagram generalizing the preparation of T-MXene@C [44]. (**G**) Low-magnification TEM [44].

2.2.4. Other Synthesis Strategies

In addition to the synthetic methods involved above, there are some other synthetic strategies to prepare MXenes-based binary composite sodium-ion battery anode materials [45,46], such as chemical vapour deposition (CVD) and anodic oxidation. Shen et al. [47] successfully synthesised TiC/C core/shell nanowire arrays on Ti_6Al_4V substrates using a modified one-step chemical vapour deposition (CVD) method. The prepared TiC/C nanowire arrays have a core/shell structure and a porous structure, which increase the contact and active area, provide good buffering capacity against volume changes, and enable fast electron/ion transfer. Zhang et al. [48] successfully synthesised amorphous vanadium oxide/V_2C MXenes (a-VO_x/V_2C) nano by anodic oxidation of multilayers of V_2CT_x at a constant voltage in aqueous electrolyte hybrids. The reversible capacity was as high as 307 mAh g^{-1} at 50 mA g^{-1}, and the multiplicative capacity was as high as 96 mAh g^{-1} at 2000 mA g^{-1}.

2.3. Design and Synthesis of MXene-Based Ternary Composites

Based on the synthetic basis of MXenes-based binary composites, researchers have designed and constructed MXenes-based ternary composites in anticipation of obtaining anode materials for sodium-ion batteries with better electrochemical properties. Cao et al. [49] then designed a unique microbial electrostatic assembly method based on the traditional electrostatic assembly method and prepared a 2D transition metal sulphide-MXene-carbon-based nanoribbon with heterogeneous structured negative electrodes (Figure 6A). This method promotes the migration and stable storage of high-capacity Na^+ by constructing a heterojunction interface with multiple surface-active sites and highly conductive main chain structure, effectively alleviating the slow kinetics of sodium-ion batteries. However, the performance of MXenes-based composites prepared by a single synthesis process often fails to reach the expectation, and multiple preparation methods also need to be used together. Yuan et al. [50] used the template method and the electrostatic assembly method to prepare the Nb_2CT_x/MoS_2@CS ternary composites, which had a specific capacity of 394 mAh g^{-1}, with 74.1% capacity retention after 900 cycles at a current density of 1 A g^{-1}, with good capacity stability (Figure 6B). Li et al. [51] combined the in situ growth method and template method to assemble $Ti_3C_2T_x$ MXene nanosheets into thin-walled hollow spheres using PMMA spheres as sacrificial templates (Figure 6C), and then N-doped CoS_2 nanoparticles embedded in them were grown to obtain MXene@CoS_2/NC ternary composites. The electrochemical performance test shows that it has a high initial discharge capacity of 355 mAh g^{-1} and the capacity retention rate is around 100% after 5000 cycles (Figure 6D).

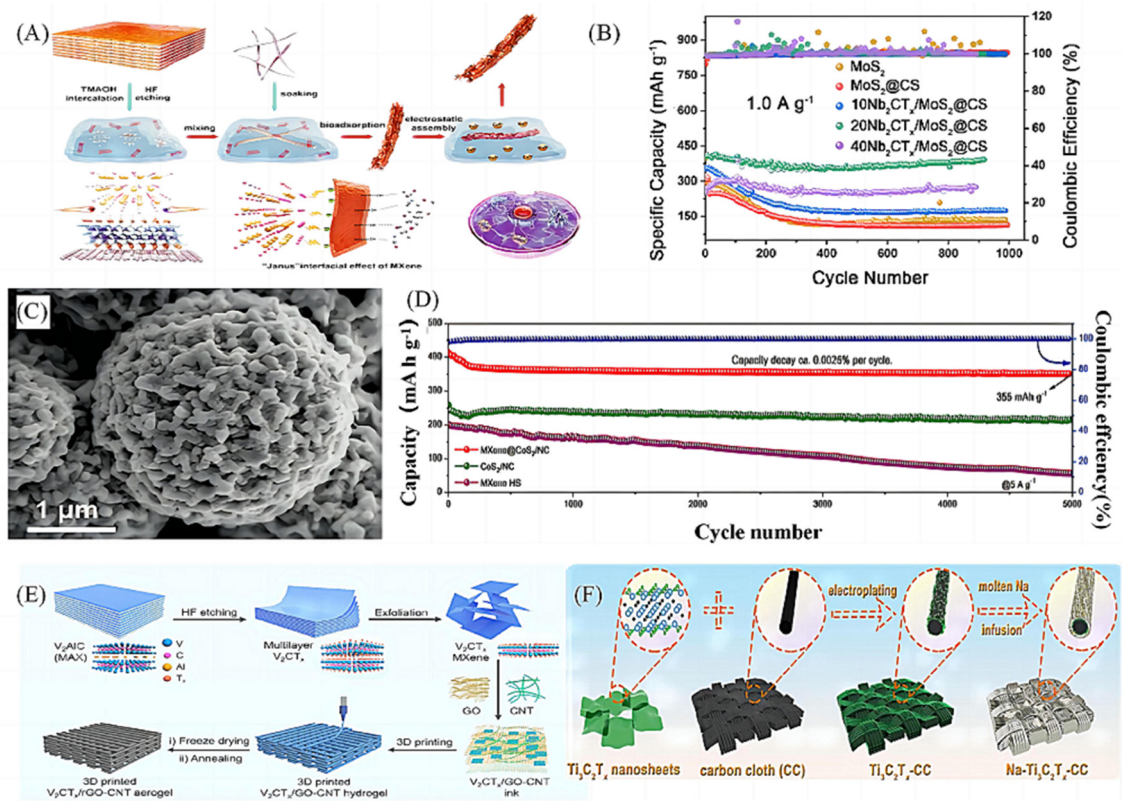


Figure 6. (**A**) Schematic illustration of transitional metal chalcogenide (TMC)on MXene coated fungal-derived carbonaceous nanoribbon (CNRib) heterostructure (TMC@MXene@CNRib) [49]. (**B**) Cycling performances at current density of 1 A g^{-1} [50]. (**C**) SEM images of MXene@CoS_2/NC spheres in sequence [51]. (**D**) Long-term cycling stability of MXene@CoS_2/NC [52]. (**E**) Schematic diagram of the preparation process of a 3D-printed V2CTx/rGO-CNT microgrid aerogel electrode [52]. (**F**) Schematic diagram of fabrication procedure for $Ti_3C_2T_x$-CC skeletons and Na-$Ti_3C_2T_x$-CC metal anodes [53].

In addition to common preparation methods, some new synthesis processes have been gradually developed, and Wang et al. [52] innovatively proposed the preparation of a 3D printed V_2CT_x/rGO-CNT anode (Figure 6E). The hierarchical and porous 3D structure of this ternary composite not only maintains the relative integrity of the entire electrode structure, but also provides abundant active sites to enhance the Na ion/electron transport kinetics of sodium-ion batteries. Electrochemical performance tests showed that the anode material could maintain stable cycling for 3000 h at 2 mA cm^{-2} and 10 mAh cm^{-2} with an average Coulombic efficiency of 99.54%, as well as stable operation for 1000 h at high current densities of 5 mA cm^{-2} and 50 mAh cm^{-2}. Fang et al. [53] have also used the novel synthesis processes-coating method and melt-infusion method to obtain Na-$Ti_3C_2T_x$-CC ternary composites (Figure 6F). The composites have good anti-viscosity and machinability, which verifies the feasibility of producing flexible Na-metal electrodes and provides new possibilities to promote the practical application of sodium-ion batteries.

Table 1. Comparison of physical properties of MXene-based materials.

Serial Number	Material Composition	Preparation Method	First Charge (mAh g^{-1})	First Discharge (mAh g^{-1})	Cycling Performance	Rate Capability	References
1	S-doped $Ti_3C_2T_x$	Vacuum freeze drying	821.7	970	577 mAh g^{-1} after 500 cycles		[17]
2	S-doped $Ti_3C_2T_x$	Electrostatic self-assembly		325	135 mAh g^{-1} after 1000 cycles at 2.0 A g^{-1}	136.6 mAh g^{-1} at 5 A g^{-1}	[18]
3	S-doped mesoporous $Ti_3C_2T_x$ film	Electrostatic self-assembly		354.6	345.6 mAh cm^{-3} after 5000 cycles at 1 A g^{-1}	129.2 m Ah g^{-1} at 1 A g^{-1}	[20]
4	N-doped $Ti_3C_2T_x$	Electrostatic self-assembly	132.6	338.5	123.4 mAh g^{-1} after 5000 cycles at 1 A g^{-1}	120 mAh g^{-1} at 1 A g^{-1}	[24]
5	N-doped $Ti_3C_2T_x$	Electrostatic self-assembly		1844.7	284.2 mAh g^{-1} after 1000 cycles at 5.0 C	180.5 mAh g^{-1}at 25 C	[25]
6	VO_2/MXenes	Hydrothermal method		229.2	280.9 mAh g^{-1} after 200 cycles at 0.1 A g^{-1}	206 mAh g^{-1} at 1.6 A g^{-1}	[29]
7	$NaTi_8O_{13}/NaTiO_2$	Two-step hydrothermal method	125	162	82 mAh g^{-1} after 1900 cycles at 2.0 A g^{-1}	143 mAh g^{-1} at 0.1 A g^{-1}	[30]
8	$MoSe_2$/MXene	Hydrothermal method combined with thermal annealing process	578	826	384 mAh g^{-1} after 400 cycles at 2.0 A g^{-1}	490 mAh g^{-1} at 1.0 A g^{-1}	[31]
9	$SnS/Ti_3C_2T_x$	Hydrothermal method combined with thermal annealing process	348.4	495.0	320 mAg^{-1} after 50 cycles at 500 mAg^{-1}	255.9 mAh g^{-1} at 1000 mA g^{-1}	[32]
10	$CoNiO_2$/MXene	Hydrothermal method combined with thermal annealing process		463	223 mAh g^{-1} after 140 cycles at 0.1 A g^{-1}	188 mAh g^{-1} at 0.3 A g^{-1}	[33]
11	VO_2-NTs/Ti_3C_2	Electrostatic self-assembly	1164	2132	516 mAh g^{-1} after 2000 cycles at 5.0 A g^{-1}	703 mAh g^{-1} at 10.0 A g^{-1}	[35]
12	$Ti_3C_2T_x$/CNT	Electrostatic self-assembly	179	501	120 mAh g^{-1} after 500 cycles at 0.1 A g^{-1}		[36]
13	PDDA-BP/Ti_3C_2	Electrostatic self-assembly	1780	2588	1112 mAh g^{-1} after 500 cycles at 0.1 A g^{-1}	560 mAh g^{-1} at 1 A g^{-1}	[37]
14	TiO_2@$Ti_3C_2T_x$	Electrostatic self-assembly	233.9	497.1	116 mAh g^{-1} after 5000 cycles at 0.96 A g^{-1}	177 mAh g^{-1} at 0.12 A g^{-1}	[40]
15	M-SnP-In	In situ synthesis		438.2	436.6 $mAhg^{-1}$ after 1500 cycles at 2 Ag^{-1}	438.2 $mAhg^{-1}$ at 15 A g^{-1}	[41]

Table 1. *Cont.*

Serial Number	Material Composition	Preparation Method	First Charge (mAh g^{-1})	First Discharge (mAh g^{-1})	Cycling Performance	Rate Capability	References
16	T-MXene@C	In situ synthesis	580.6		499.4 mAh g^{-1} after 200 cycles at 0.2 C	478 mAh g^{-1} at 0.2 C (1 C = 320 mA g^{-1})	[44]
17	a-VO_x/V_2C	In situ synthesis		161	54 mAh g^{-1} after 1800 cycles at 2000 mA g^{-1}	96 mAh g^{-1} at 2 Ah g^{-1}	[48]
18	$Cu_{1.75}Se$—MXene—CNRib	Microbial electrostatic assembly	744.2	1353.1	305.6 mAh g^{-1} after 400 cycles at 1.0 A g^{-1}	435.3, 356.2, 315.7, 274.3, 232.6, and 161.3 mAh g^{-1} at 0.1 to 5.0 A g^{-1}	[49]
19	Nb_2CT_x/MoS_2/CS	Electrostatic self-assembly method + template method		1270	526 mAh g^{-1} after 100 cycles at 0.1 A g^{-1} 394 mAh g^{-1} after 900 cycles at 1 A g^{-1}	196 mAh g^{-1} at 20 A g^{-1}	[50]
20	MXene@CoS_2/NC	In situ growth method + template method	660	885	620 mAhg^{-1} after 200 cycles at 0.2 A g^{-1}	708, 614, 551, 438, and 394 mAh g^{-1} at 0.2, 0.5, 1, 2, and 5 A g^{-1}	[51]

3. First-Principles Study of Anode Materials for MXenes-Based Sodium-Ion Batteries

The first principles based on density functional theory can simulate the kinetics of electrochemical reactions from the atomic level, which helps to understand and analyse the relevant energy storage mechanism of battery materials, and also provides a theoretical basis for the design of new battery materials, which is one of the important research tools in the field of energy storage devices. In the research process of MXenes-based anode materials for sodium-ion batteries, many researchers have conducted many studies on the electronic structure of MXene materials, the structure and physical and chemical properties of element-doped MXene materials and MXenes-based composites before and after modification, which have made great contributions to the understanding of the role of MXene materials in sodium-ion batteries.

All first-principles calculations were performed by the Vienna Ab initio Simulation Package (VASP). We chose projected-augmented-wave method (PAW) to describe the electron-ion interaction. The exchange–correlation interaction functional is the generalized gradient approximation (GGA) in the Perdew–Burke–Ernzerhof (PBE) functional.

3.1. MXenes Theoretical Computational Study of the Electronic Structure of the Material

Er et al. [54] conducted a first-principles study of the electronic structure of sodium ions on Ti_3C_2 in order to understand the differences in their adsorption on Ti_3C_2. Through the calculation of Na adsorption energy (Figure 7A), the adsorption energy was found to be only 4.40 eV, and combined with the results of density of states simulation of Ti_3C_2 before and after Na adsorption, the diffusion barrier of Na^+ was 0.096 eV (Figure 7B), which indicated that Ti_3C_2 is a promising anode material for sodium-ion batteries. The basic mechanism for the MXene column effect to enhance the electrode performance of sodium-ion batteries is still unclear; based on this, Dai et al. [55] investigated the effects of different MXene interlayer stacking methods on the adsorption, diffusion and mechanical properties of Na atoms by employing the first nature principle with two typical MXenes as the research objects. It was found that for both $Ti_3C_2O_2$ and Ti_2CO_2 configurations, the diffusion energy barriers of Na were greatly reduced when the C-Ti stacking mode was adopted (Figure 7C,D). This provides a useful theoretical basis for understanding the MXene column effect and contributes to the development of anode materials for sodium-ion batteries. This was followed by a first-principles study of the Na storage capacity of $Ti_3C_2T_x$ by Bai et al. [56], which, after comprehensive calculations for all configurations of Eads2, extended the calculations to their theoretical capacities and obtained the optimal capacity-to-structure ratios in the stacked structure. The calculated CMNa value can be increased from 218.32 mAh g^{-1} to 413.13 mAh g^{-1}, which is in good agreement with the previously reported value of 413.0 mAh g^{-1}. The analysis of the optimal capacity-to-structure ratio shows that the increase in layer spacing favours the increase in MXene capacity, which provides a theoretical basis for achieving high-capacity sodium storage behaviour.

3.2. Theoretical Computational Study of Elementally Doped MXenes Materials

Using elemental doping as one of the common modification means, researchers have carried out a lot of studies on the first nature principle of elementally doped MXene materials. Bao et al. [17] experimentally demonstrated that the S-modified Ti_3C_2 material has a strong adsorption of Na_2S_n in the Na–S cell. Based on this, Lu et al. [57] used a first-principles simulation to calculate the chemical properties and bond strengths between S-modified Ti_3C_2 and Na_2Se_n, which showed that S-doped Ti_3C_2 has strong anchoring and trapping effects on Na_2Se_n (Figure 8A). S-doped MXenes not only improve the chemical bonding energy and van der Waals force on Na_2Se_n, but also, more importantly, the joint action of S-doped MXene materials and the nano-scaled Na_2Se_n together can maximize the surface or near-surface charge storage of MXene materials, which is conducive to improving the charging and discharging capacity of sodium-ion batteries. Wang et al. [58], on the other hand, systematically investigated the performance of sulphur-functionalized

MXenes as anode materials for sodium-ion batteries. The structural, kinetic and electronic properties of S-functionalized Ti_2C single molecule membranes (Ti_2CS_2) were comprehensively investigated by first-principles calculations. The results show that the Ti_2CS_2 monolayers have not only good kinetic stability, but also metallic properties, thus ensuring excellent structural stability and electronic conductivity. Meanwhile the low diffusion barrier of Na^+ and multilayer stable adsorption ensure the excellent capacity of Ti_2CS_2 monolayers in sodium-ion (935.57 mAh g^{-1}) batteries, which is a theoretical basis for the design of high-capacity sodium-ion batteries. Liao et al. [59] investigated the effect of N doping on the electrical conductivity of Ti_2C and Ti_3C_2 MXene materials before and after N doping using first-principles calculations. The results show that N doping can significantly improve the electrical conductivity of Ti_2C and Ti_3C_2 (Figure 8B), while both Ti_2C and Ti_3C_2 exhibit metallicity at different N doping concentrations, which offers the possibility of their further application in sodium-ion batteries. In order to achieve the performance of fast charging and long cycling in sodium-ion batteries, Xia et al. [60] explored the effect of N doping on the electronic structure of Ti_3C_2 using first-principles calculations. The results show that N atom doping induces charge redistribution and the formation of active sites in the MXene material, and at the same time improves the electronic conductivity of $Ti_3C_2O_{1.83}N_{0.17}$,which suggests the feasibility of realising high-performance sodium-ion electrodes based on the MXene material at room temperature.

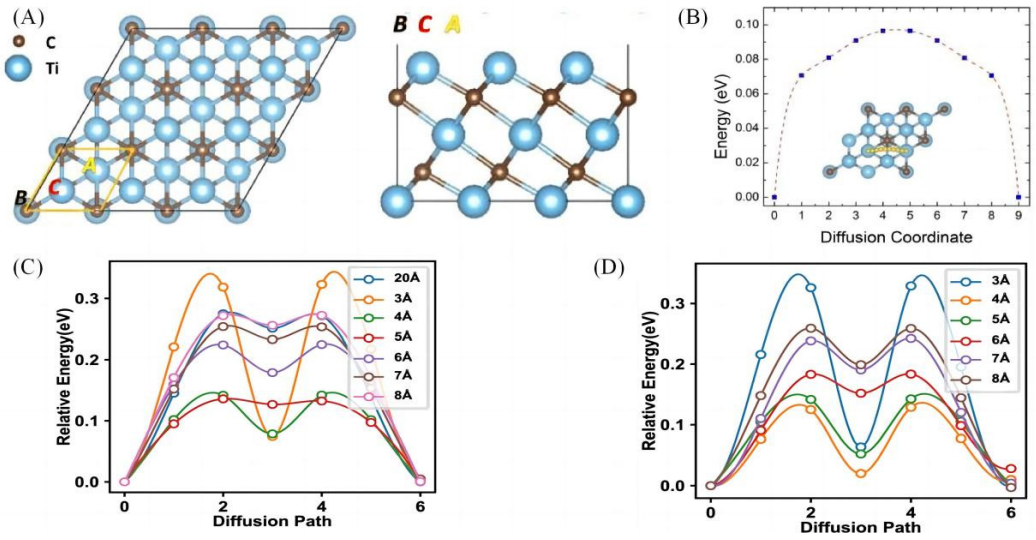


Figure 7. (**A**) Schematic diagram showing the crystal structure of a Ti_3C_2 monolayer with top and side view. The large blue balls represent Ti atoms and the small brown balls represent C atoms. The highlighted unit cell indicates the high-symmetry A, B, and C adatom [54]. (**B**) Schematic representation of the top view of the energetically optimized migration pathways and the corresponding diffusion barrier profiles of Na [54]. (**C**) Distribution of the energy barrier profiles of Na diffusion under Different interlayer spacings in C–Ti stacking of $Ti_3C_2O_2$ [55]. (**D**) Distribution of the energy barrier profiles of Na diffusion under Different interlayer spacings in C-Ti stacking of C-Tistacking of Ti_2CO_2 [55].

In addition to the common studies on N and S-element-doped MXene materials, researchers have also investigated the first principles of other element-doped MXene materials. Zhao et al. [37] investigated the relaxation process when Na was added to the surface functional groups (-F, -O, and -OH), and by comparing the binding energy as well as the charge densities (Figure 8C), the researchers found that the intercalated Na^+ first binds to the BP nanoparticles and then undergoes mixed adsorption on -F, -O and -P, which consequently reduces the binding energy and thus facilitates the diffusion of Na^+ and charge transfer. Kajiyama et al. [61] have revealed that $Ti_3C_2T_x$ exhibits a reversible Na^+ embedding/de-embedding behaviour into/from the interlayer space in the

non-Na^+ electrolyte without a structural reason for the structural changes. The interlayer distance was maintained throughout the sodiation/desorption process due to the column-supporting effect of the captured Na^+ and the swelling effect of the permeated solvent molecules between the $Ti_3C_2T_x$ sheets, achieving reversible embedding/de-embedding of Na^+, and thus no substantial structural changes occurred during the electrochemical reaction. For these reasons, $Ti_3C_2T_x$ shows good capacity retention as well as excellent multiplicity in 100 cycles (Figure 8D), making it a promising anode material for sodium-ion batteries.

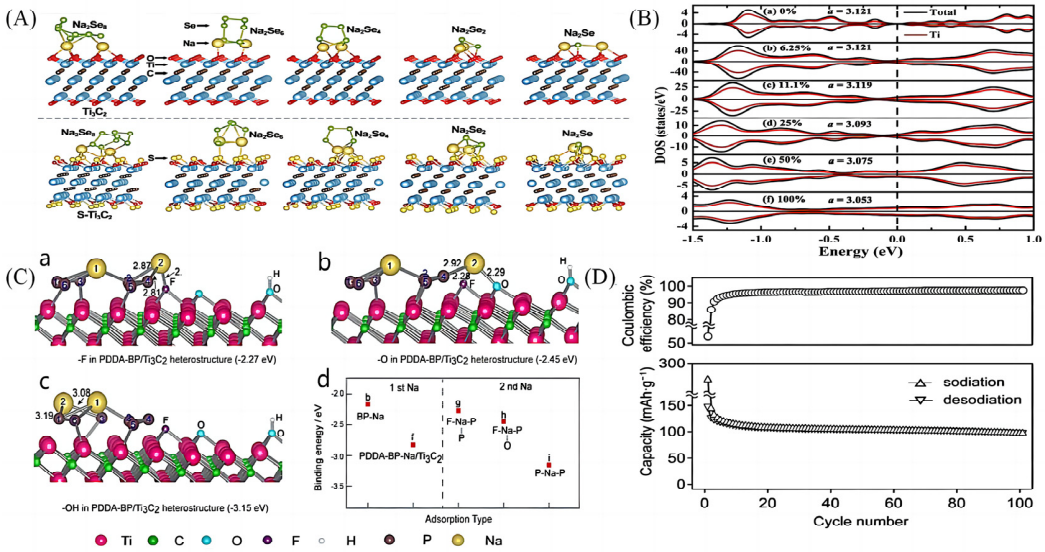


Figure 8. (**A**) Adsorption configurations of Na_2Se_n (n = 8, 6, 4, 2, and 1, respectively) on the surface) and pristine Ti_3C_2 [57]. (**B**) Total and partial density of states (DOS) of N-doped Ti_2C monolayer with doping concentrations of (a) 0%, (b) 6.25%, (c) 11.1%, (d) 25%, (e) 50% and (f) 100%, i.e., Ti_2N monolayer. a is the lattice constant for a per unit cell at different concentrations of nitrogen [59]. (**C**) (**a**–**c**) the most stable adsorption configurations for another Na adsorption on top of functional groups in the heterostructures, such as -F, -O and -OH. (**d**) The calculated binding energies for Na adsorption on the surface of BP nanoparticle or PDDA-BP/Ti_3C_2 heterostructures with different surface functional groups [37]. (**D**) Cycle performance for $Ti_3C_2T_x$ at 20 mA g^{-1} [61].

3.3. Theoretical Computational Study of MXenes Matrix Composites

Composite modification of MXene materials is also a good means of enhancing the properties, so many researchers have also focused on first-principles-related studies on MXenes-based composites. Zhao et al. [37] studied the interaction between Na and BP nanoparticles by first-principles calculations, and found that the interaction between Na and BP nanoparticles was significantly altered by comparing the Na-BP system and the PDDA-BP/Ti_3C_2 system before and after the relaxation process in terms of conformation, binding energy and charge density, it was found that Ti_3C_2 nanosheets significantly changed the sodic state of BP nanoparticles, which made it easier for them to obtain electrons from Na, facilitated the sodic process, and improved the sodium storage performance of the MXenes-based anode materials. Cao et al. [49] have conducted first-principles computational studies on the diffusion at the interface of MSe-MXenes-CNRib heterostructure behaviour, which was investigated by first-principles calculations. By studying the density of states of the ternary heterostructure, the adsorption energy, the difference in charge distribution of the Na adsorption heterostructure, and the energy distribution state of diffusion, it was not only confirmed that the synergistic effect would promote the adsorption and diffusion of Na ions to a certain extent, but it was also found that the heterostructure was capable of high-capacity storage of Na ions under different multiplicity conditions. Liu et al. [35] created a rational construction of the MXenes-based composite system based on the density functional theory, and the VO_2 nanotubes (VO_2-NTs) and $Ti_3C_2T_x$ MXenes were composed

into the VO_2-NTs/Ti_3C_2 negative electrode material with a multidimensional cross-linking structure. Relevant theoretical calculations show that the rich multidimensional channels of the composite reduce the diffusion impedance of Na^+, while the enhanced intrinsic conductivity and highly rigid structure solve the problems of poor cycling stability and multiplicity performance of VO_2 due to the large volume change, which promotes the further practical application of sodium-ion batteries.

4. Conclusions

This review summarises the research efforts and developments in recent years on the design and synthesis strategies as well as first-principles studies of MXenes-based anode materials for sodium-ion batteries, detailing their numerous achievements in the field of sodium-ion batteries, and providing new possibilities for promoting the further practicalisation of sodium-ion batteries. In spite of the great progress made, there are still several key issues that have not been resolved in the research on the design and synthesis strategies and first principles of MXene-based anode materials for sodium-ion batteries, as shown below:

(1) Currently, the main method to obtain MXenes is still acid etching, which is characterised by low yield and high risk. Therefore, there is an urgent need for environmentally friendly, safe, efficient and high-quality methods, such as CVD or PVD, to synthesize MXenes with a controllable number of layers, adjustable surface groups, increased layer spacing and excellent quality. In addition, there is a need to optimize the existing synthesis methods and conduct in-depth research on the generation mechanism, which can be used to promote the practical large-scale industrial production of MXenes and MXenes-based materials.

(2) As mentioned earlier, the surface chemistry of MXenes may significantly affect the properties of MXenes-based materials. Different etchants can produce groups with different surface chemistries, but the precise surface chemistry of MXenes and the interactions between the surface groups and the materials are still not well understood. In addition, it was shown that bare/-O capped MXenes have better physicochemical properties. Therefore, more studies are needed to modulate the surface chemistry and explore its application in electrochemical storage.

(3) Another major problem with MXenes is their stability. The interlayer structure of an MXene is unstable under room temperature conditions, which can easily lead to the problem of heavy stacking, which seriously hinders the long-term development of MXenes-based materials. To alleviate this situation, efforts can be focused on rational structural design and precise morphological control of electrodes, such as 3D porous structure, aerogel and coating technology.

(4) Theoretical studies must take into account the inhomogeneous and incomplete mixed coverage of surface groups and MXene-stacked multilayers in order to accurately predict their properties and thus guide experiments. It is thus necessary to combine theoretical calculations with advanced computations, including machine learning, classical molecular dynamics and high-throughput calculations, to fully understand the surface chemistry and interfaces of MXenes-based materials. In addition, relevant theoretical models as well as computational software and hardware should be further developed to narrow the gap between theoretical predictions and experimental results.

In summary, MXenes are one of the electrode materials with great potential for development in the field of energy storage devices, but they still face great challenges in moving from the laboratory research stage to the industrial application stage. This requires researchers to conduct sufficient practical studies to improve the knowledge and understanding of this class of materials in order to explore and exploit its material advantages and to promote the commercial application of MXenes.

Author Contributions: D.S. was responsible for most of the work, such as writing the main content of the article, drawing, and data inquiry; H.Z. made a summary and statistical analysis of the progress of relevant materials. He applied statistics and other techniques to analyse or synthesize the characteristic information of the research materials, guided and gave the main line of the review, and as the co-author of the article, he made significant contributions to the large length of the article summary and the progress of the timeline; J.Z. was responsible for part of the content writing, drawing and data query. Y.Z. was responsible for the idea of the entire paper, paper revision and other work. All authors have read and agreed to the published version of the manuscript.

Funding: This work was financially supported by the Hebei Province Natural Science Foundation of Iron and Steel Joint Fund: (No. E2021209002), and it was also supported by Project of Tangshan Science and Technology Bureau (No. 21130211D, 22130215H).

Institutional Review Board Statement: Not applicable.

Informed Consent Statement: Not applicable.

Data Availability Statement: All relevant data are provided in the article.

Conflicts of Interest: The authors declare no conflict of interest.

Sample Availability: Not applicable.

References

1. Li, Y.; Guo, J.; Pedersen, K.; Gurevich, L.; Stroe, D.-I. Investigation of multi-step fast charging protocol and aging mechanism for commercial NMC/graphite lithium-ion batteries. *J. Energy Chem.* **2023**, *80*, 237–246. [CrossRef]
2. Li, Y.; Li, Y.; Zhang, L.; Tao, H.; Li, Q.; Zhang, J.; Yang, X. Lithiophilicity: The key to efficient lithium metal anodes for lithium batteries. *J. Energy Chem.* **2023**, *77*, 123–136. [CrossRef]
3. Wang, P.; Guo, Y.-J.; Chen, W.-P.; Duan, H.; Ye, H.; Yao, H.-R.; Yin, Y.-X.; Cao, F.-F. Self-supported hard carbon anode from fungus-treated basswood towards sodium-ion batteries. *Nano Res.* **2022**, *16*, 3832–3838. [CrossRef]
4. Tong, Y.; Wu, Y.; Liu, Z.; Yin, Y.; Sun, Y.; Li, H. Fabricating multi-porous carbon anode with remarkable initial coulombic efficiency and enhanced rate capability for sodium-ion batteries. *Chin. Chem. Lett.* **2023**, *34*, 107443. [CrossRef]
5. Zhou, D.; Ning, D.; Wang, J.; Liu, J.; Zhang, G.; Xiao, Y.; Zheng, J.; Li, Y.; Li, J.; Liu, X. Clarification of underneath capacity loss for O_3-type Ni, co free layered cathodes at high voltage for sodium ion batteries. *J. Energy Chem.* **2023**, *77*, 479–486. [CrossRef]
6. Xu, Y.; Xiong, W.; Huang, J.; Tang, X.; Wang, H.; Liu, W.; Xiao, D.; Guo, Y.; Zhang, Y. Pressure-induced growth of coralloid-like FeF_2 nanocrystals to enable high-performance conversion cathode. *J. Energy Chem.* **2023**, *79*, 291–300. [CrossRef]
7. Liu, C.; Lu, Q.; Gorbunov, M.V.; Omar, A.; Gonzalez Martinez, I.G.; Zhao, P.; Hantusch, M.; Permana, A.D.C.; He, H.; Gaponik, N.; et al. Ultrasmall CoS nanoparticles embedded in heteroatom-doped carbon for sodium-ion batteries and mechanism explorations via synchrotron X-ray techniques. *J. Energy Chem.* **2023**, *79*, 373–381. [CrossRef]
8. Pomerantseva, E.; Bonaccorso, F.; Feng, X.; Cui, Y.; Gogotsi, Y. Energy storage: The future enabled by nanomaterials. *Science* **2019**, *366*, 969–981. [CrossRef]
9. Pomerantseva, E.; Gogotsi, Y. Two-dimensional heterostructures for energy storage. *Nat. Energy* **2017**, *2*, 17089. [CrossRef]
10. Alhabeb, M.; Maleski, K.; Mathis, T.S.; Sarycheva, A.; Hatter, C.B.; Uzun, S.; Levitt, A.; Gogotsi, Y. Selective Etching of Silicon from Ti_3SiC_2 (MAX) To Obtain 2D Titanium Carbide (MXene). *Angew Chem. Int. Ed. Engl.* **2018**, *57*, 5444–5448. [CrossRef]
11. Yang, X.; Wang, Q.; Zhu, K.; Ye, K.; Wang, G.; Cao, D.; Yan, J. 3D Porous Oxidation-Resistant MXene/Graphene Architectures Induced by In Situ Zinc Template toward High-Performance Supercapacitors. *Adv. Funct. Mater.* **2021**, *31*, 2101087. [CrossRef]
12. Naguib, M.; Mashtalir, O.; Carle, J.; Presser, V.; Lu, J.; Hultman, L.; Gogotis, Y.; Barsoum, M.W. Two-dimensional transition metal carbides. *ACS Nano* **2012**, *6*, 1322–1331. [CrossRef]
13. Zhan, C.; Naguib, M.; Lukatskaya, M.; Kent, P.R.C.; Gogotsi, Y.; Jiang, D.E. Understanding the MXene Pseudocapacitance. *Phys. Chem. Lett.* **2018**, *9*, 1223–1228. [CrossRef] [PubMed]
14. Xie, Y.; Dall'Agnese, Y.; Naguib, M.; Gogotis, Y.; Barsoum, M.W.; Zhuang, H.L.; Kent, P.R.C. Prediction and Characterization of MXene Nanosheet Anodes for Non-Lithium-Ion Batteries. *ACS Nano* **2014**, *8*, 9606–9615. [CrossRef]
15. Ma, P.; Fang, D.; Liu, Y.; Shang, Y.; Shi, Y.; Yang, H.Y. MXene-Based Materials for Electrochemical Sodium-Ion Storage. *Adv. Sci.* **2021**, *8*, 2003185. [CrossRef] [PubMed]
16. Zhao, L.; Sun, S.; Lin, J.; Zhong, L.; Chen, L.; Guo, J.; Yin, J.; Alshareef, H.N.; Qiu, X.; Zhang, W. Defect Engineering of Disordered Carbon Anodes with Ultra-High Heteroatom Doping Through a Supermolecule-Mediated Strategy for Potassium-Ion Hybrid Capacitors. *Nano-Micro Lett.* **2023**, *15*, 41. [CrossRef] [PubMed]
17. Bao, W.; Shuck, C.E.; Zhang, W.; Guo, X.; Gogotsi, Y.; Wang, G. Boosting Performance of Na-S Batteries Using Sulfur-Doped $Ti_3C_2T(x)$ MXene Nanosheets with a Strong Affinity to Sodium Polysulfides. *ACS Nano* **2019**, *13*, 11500–11509. [CrossRef]
18. Sun, S.; Xie, Z.; Yan, Y.; Wu, S. Hybrid energy storage mechanisms for sulfur-decorated Ti_3C_2 MXene anode material for high-rate and long-life sodium-ion batteries. *Chem. Eng. J.* **2019**, *366*, 460–467. [CrossRef]

19. Li, J.; Yan, D.; Hou, S.; Li, Y.; Lu, T.; Yao, Y.; Pan, L. Improved sodium-ion storage performance of $Ti_3C_2T_x$ MXenes by sulfur doping. *J. Mater. Chem. A* **2018**, *6*, 1234–1243. [CrossRef]
20. Li, G.; Lian, S.; Song, F.; Chen, S.; Wu, Z.; Xie, X.; Zhang, N. Surface Chemistry and Mesopore Dual Regulation by Sulfur-Promised High Volumetric Capacity of $Ti_{(3)}C_{(2)}T_{(x)}$ Films for Sodium-Ion Storage. *Small* **2021**, *17*, 2103626. [CrossRef]
21. Lu, C.; Yang, L.; Yan, B.; Sun, L.; Zhang, P.; Zhang, W.; Sun, Z. Nitrogen-Doped Ti_3C_2 MXene: Mechanism Investigation and Electrochemical Analysis. *Adv. Funct. Mater.* **2020**, *30*, 2000852. [CrossRef]
22. Ji, X.; Chen, X.; Zhang, L.; Meng, C.; He, Y.; Zhang, X.; Wang, Z.; Yu, R. Anchoring nitrogen-doped Co_2P nanoflakes on $NiCo_2O_4$ nanorod arrays over nickel foam as high-performance 3D electrode for alkaline hydrogen evolution. *Green Energy Environ.* **2023**, *8*, 470–477. [CrossRef]
23. Gao, M.; Li, J.; Wang, Y.; Liang, W.; Yang, Z.; Chen, Y.; Deng, W.; Wang, Z.; Ao, T.; Chen, W. Flexible nitrogen-doped carbon nanofiber-reinforced hierarchical hollow iron oxide nanorods as a binder-free electrode for efficient capacitive deionization. *Desalination* **2023**, *549*, 116360. [CrossRef]
24. Jin, X.; Zhang, W.; Liu, S.; Zhang, T.; Song, Z.; Shao, W.; Mao, R.; Yao, M.; Jian, X.; Hu, F. Highly stable $Ti_3C_2T_x$ MXene-based sandwich-like structure via interfacial self-assembly of nitrogen-rich polymer network for superior sodium-ion storage performance. *Chem. Eng. J.* **2023**, *451*, 138763. [CrossRef]
25. Fan, Z.; Wei, C.; Yu, L.; Xia, Z.; Cai, J.; Tian, Z.; Zou, G.; Dou, S.; Sun, J. 3D Printing of Porous Nitrogen-Doped Ti_3C_2 MXene Scaffolds for High-Performance Sodium-Ion Hybrid Capacitors. *ACS Nano* **2020**, *14*, 867–876. [CrossRef] [PubMed]
26. Lim, H.; Yu, S.; Choi, W.; Kim, S.-O. Hierarchically Designed Nitrogen-Doped MoS_2/Silicon Oxycarbide Nanoscale Heterostructure as High-Performance Sodium-Ion Battery Anode. *Acs Nano* **2021**, *15*, 7409–7420. [CrossRef]
27. Xia, Q.; Liang, Y.; Lin, Z.; Wang, S.; Lai, W.; Yuan, D.; Dou, Y.; Gu, Q.; Wang, J.; Liu, H.; et al. Confining Ultrathin 2D Superlattices in Mesoporous Hollow Spheres Renders Ultrafast and High-Capacity Na-Ion Storage. *Adv. Energy Mater.* **2020**, *10*, 2001033. [CrossRef]
28. Liu, Y.; Fang, Y.; Zhao, Z.; Yuan, C.; Lou, X. A Ternary Fe1-xS@Porous Carbon Nanowires/Reduced Graphene Oxide Hybrid Film Electrode with Superior Volumetric and Gravimetric Capacities for Flexible Sodium Ion Batteries. *Adv. Energy Mater.* **2019**, *9*, 1803052. [CrossRef]
29. Wu, F.; Jiang, Y.; Ye, Z.; Huang, Y.; Wang, Z.; Li, S.; Mei, Y.; Xie, M.; Li, L.; Chen, R. A 3D flower-like VO_2/MXene hybrid architecture with superior anode performance for sodium ion batteries. *J. Mater. Chem. A* **2019**, *7*, 1315–1322. [CrossRef]
30. Sun, X.; Tan, K.; Liu, Y.; Zhang, J.; Hou, L.; Yuan, C. In-situ growth of hybrid $NaTi_8O_{13}$/$NaTiO_2$ nanoribbons on layered MXene Ti_3C_2 as a competitive anode for high-performance sodium-ion batteries. *Chin. Chem. Lett.* **2020**, *31*, 2254–2258. [CrossRef]
31. Xu, E.; Zhang, Y.; Wang, H.; Zhu, Z.; Quan, J.; Chang, Y.; Li, P.; Yu, D.; Jiang, Y. Ultrafast kinetics net electrode assembled via $MoSe_2$/MXene heterojunction for high-performance sodium-ion batteries. *Chem. Eng. J.* **2020**, *385*, 123839. [CrossRef]
32. Zhang, Y.; Guo, B.; Hu, L.; Xu, Q.; Li, Y.; Liu, D.; Xu, M. Synthesis of SnS nanoparticle-modified MXene ($Ti_3C_2T_x$) composites for enhanced sodium storage. *J. Alloys Compd.* **2018**, *732*, 448–453. [CrossRef]
33. Tao, M.; Zhang, Y.; Zhan, R.; Guo, B.; Xu, Q.; Xu, M. A chemically bonded $CoNiO_2$ nanoparticles/MXene composite as anode for sodium-ion batteries. *Mater. Lett.* **2018**, *230*, 173–176. [CrossRef]
34. Wang, J.; Du, C.F.; Xue, Y.; Tan, X.; Kang, J.; Gao, Y.; Yu, H.; Yan, Q. MXenes as a versatile platform for reactive surface modification and superior sodium-ion storages. *Exploration* **2021**, *1*, 20210024. [CrossRef]
35. Liu, H.; He, P.; Cao, J.; Duan, T.; Kong, Q.; Yao, W. Multidimensional VO_2 nanotubes/Ti_3C_2 MXene composite for efficient electrochemical lithium/sodium-ion storage. *J. Power Sources* **2022**, *521*, 230946. [CrossRef]
36. Xie, X.; Zhao, M.-Q.; Anasori, B.; Maleski, K.; Ren, C.E.; Li, J.; Byles, B.W.; Pomerantseva, E.; Wang, G.; Gogotsi, Y. Porous heterostructured MXene/carbon nanotube composite paper with high volumetric capacity for sodium-based energy storage devices. *Nano Energy* **2016**, *26*, 513–523. [CrossRef]
37. Zhao, R.; Qian, Z.; Liu, Z.; Zhao, D.; Hui, X.; Jiang, G.; Wang, C.; Yin, L. Molecular-level heterostructures assembled from layered black phosphorene and Ti_3C_2 MXene as superior anodes for high-performance sodium ion batteries. *Nano Energy* **2019**, *65*, 104037. [CrossRef]
38. Wu, Y.; Nie, P.; Wu, L.; Dou, H.; Zhang, X. 2D MXene/SnS_2 composites as high-performance anodes for sodium ion batteries. *Chem. Eng. J.* **2018**, *334*, 932–938. [CrossRef]
39. Dong, X.; Zhao, R.; Sun, B.; Zhang, T.; Wang, B.; He, Y.; Gao, T.; Chao, D.; Zhou, G. Confining homogeneous $Ni_{0.5}Co_{0.5}Se_2$ nanoparticles in Ti_3C_2T MXene architectures for enhanced sodium storage performance. *Appl. Surf. Sci.* **2022**, *605*, 154847. [CrossRef]
40. Guo, X.; Zhang, J.; Song, J.; Wu, W.; Liu, H.; Wang, G. MXene encapsulated titanium oxide nanospheres for ultra-stable and fast sodium storage. *Energy Storage Mater.* **2018**, *14*, 306–313. [CrossRef]
41. Tang, J.; Peng, X.; Lin, T.; Huang, X.; Luo, B.; Wang, L. Confining ultrafine tin monophosphide in $Ti_3C_2T_x$ interlayers for rapid and stable sodium ion storage. *eScience* **2021**, *1*, 203–211. [CrossRef]
42. Ding, Y.; Chen, Y.; Xu, N.; Lian, X.; Li, L.; Hu, Y.; Peng, S. Facile Synthesis of $FePS_{(3)}$ Nanosheets@MXene Composite as a High-Performance Anode Material for Sodium Storage. *Nanomicro Lett.* **2020**, *12*, 54.
43. Ming, K.; Zhang, Z.; Li, H. In situ growth of $NaTiO_2$ nanotubes on $Ti_3C_2F_x$ for enhanced sodium ion batteries. *Mater. Lett.* **2022**, *309*, 131457. [CrossRef]

44. Zhang, P.; Soomro, R.A.; Guan, Z.; Sun, N.; Xu, B. 3D carbon-coated MXene architectures with high and ultrafast lithium/sodium-ion storage. *Energy Storage Mater.* **2020**, *29*, 163–171. [CrossRef]
45. Zhao, M.-Q.; Trainor, N.; Ren, C.E.; Torelli, M.; Anasori, B.; Gogotsi, Y. Scalable manufacturing of large and flexible sheets of MXene/graphene hetero-structures. *Adv. Mater. Technol.* **2019**, *4*, 1800639.
46. Zhang, T.; Jiang, X.; Li, G.; Yao, Q.; Lee, J.Y. A Red-Phosphorous-Assisted Ball-Milling Synthesis of Few-Layered Ti_3C_2Tx(MXene) Nanodot Composite. *ChemNanoMat* **2018**, *4*, 56–60.
47. Shen, Y.; Li, Y.; Deng, S.; Pan, G.; Xiong, Q.; Ding, X.; Lu, Y.; Liu, Q.; Xia, X.; Wang, X.; et al. TiC/C core/shell nanowires arrays as advanced anode of sodium ion batteries. *Chin. Chem. Lett.* **2020**, *31*, 846–850. [CrossRef]
48. Zhang, W.; Peng, J.; Hua, W.; Liu, Y.; Wang, J.; Liang, Y.; Lai, W.; Jiang, Y.; Huang, Y.; Zhang, W.; et al. Architecting Amorphous Vanadium Oxide/MXene Nanohybrid via Tunable Anodic Oxidation for High-Performance Sodium-Ion Batteries. *Adv. Energy Mater.* **2021**, *11*, 2100757. [CrossRef]
49. Cao, J.; Li, J.; Li, D.; Yuan, Z.; Zhang, Y.; Shulga, V.; Sun, Z.; Han, W. Strongly Coupled 2D Transition Metal Chalcogenide-MXene-Carbonaceous Nanoribbon Heterostructures with Ultrafast Ion Transport for Boosting Sodium/Potassium Ions Storage. *Nanomicro Lett.* **2021**, *13*, 113. [CrossRef]
50. Yuan, Z.; Cao, J.; Valerii, S.; Xu, H.; Wang, L.; Han, W. MXene-Bonded hollow MoS_2/Carbon sphere strategy for high-performance flexible sodium ion storage. *Chem. Eng. J.* **2022**, *430*, 132755. [CrossRef]
51. Li, Q.; Jiao, Q.; Yan, Y.; Li, H.; Zhou, W.; Gu, T.; Shen, X.; Lu, C.; Zhao, Y.; Zhang, Y.; et al. Optimized Co-S bonds energy and confinement effect of hollow MXene@CoS_2/NC for enhanced sodium storage kinetics and stability. *Chem. Eng. J.* **2022**, *450*, 137922. [CrossRef]
52. Wang, Z.; Huang, Z.; Wang, H.; Li, W.; Wang, B.; Xu, J.; Xu, T.; Zang, J.; Kong, D.; Li, X.; et al. 3D-Printed Sodiophilic $V_{(2)}CT_{(x)}$/rGO-CNT MXene Microgrid Aerogel for Stable Na Metal Anode with High Areal Capacity. *ACS Nano* **2022**, *16*, 9105–9116. [CrossRef]
53. Fang, Y.; Lian, R.; Li, H.; Zhang, Y.; Gong, Z.; Zhu, K.; Ye, K.; Yan, J.; Wang, G.; Gao, Y.; et al. Induction of Planar Sodium Growth on MXene ($Ti_{(3)}C_{(2)}T_{(x)}$)-Modified Carbon Cloth Hosts for Flexible Sodium Metal Anodes. *ACS Nano* **2020**, *14*, 8744–8753. [CrossRef] [PubMed]
54. Er, D.; Li, J.; Naguib, M.; Gogotsi, Y.; Shenoy, V.B. $Ti_{(3)}C_{(2)}$ MXene as a high capacity electrode material for metal (Li, Na, K, Ca) ion batteries. *ACS Appl. Mater. Interfaces* **2014**, *6*, 11173–11179. [CrossRef]
55. Dai, L.; Zhao, J.; Li, Q.; Chen, M.; Li, H.; Qu, K.; Li, R. Understanding the tunable sodium storage performance in pillared MXenes: A first-principles study. *Phys. Chem. Chem. Phys.* **2022**, *24*, 27184–27194. [CrossRef]
56. Bai, L.-N.; Kong, L.-Y.; Wen, J.; Ma, N.; Gao, H.; Zhang, X.-T. First-principles study of high performance lithium/sodium storage of $Ti_3C_2T_2$ nanosheets as electrode materials. *Chin. Phys. B* **2020**, *29*, 016802. [CrossRef]
57. Lu, C.; Li, A.; Li, G.; Yan, Y.; Zhang, M.; Yang, Q.; Zhou, W.; Guo, L. S-Decorated Porous $Ti_{(3)}C_{(2)}$ MXene Combined with In Situ Forming $Cu_{(2)}$ Se as Effective Shuttling Interrupter in Na-Se Batteries. *Adv. Mater.* **2021**, *33*, 2008414. [CrossRef] [PubMed]
58. Wang, Y.; Zhou, M.; Xu, L.-C.; Zhao, W.; Li, R.; Yang, Z.; Liu, R.-P.; Li, X. Achieving superior high-capacity batteries with the lightest Ti_2C MXene anode by first-principles calculations: Overarching role of S-functionate (Ti_2CS_2) and multivalent cations carrier. *J. Power Sources* **2020**, *451*, 227791. [CrossRef]
59. Liao, S.; Qin, W.; Sun, B.; Wu, M.; Xu, B. Electronic and magnetic properties in nitrogen-d oped 2D titanium carbides (MXenes): Insight from first-principles calculations. *Solid State Commun.* **2021**, *340*, 114549. [CrossRef]
60. Xia, Y.; Que, L.; Yu, F.; Deng, L.; Liang, Z.; Jiang, Y.; Sun, M.; Zhao, L.; Wang, Z. Tailoring Nitrogen Terminals on MXene Enables Fast Charging and Stable Cycling Na-Ion Batteries at Low Temperature. *Nanomicro Lett.* **2022**, *14*, 143. [CrossRef]
61. Kajiyama, S.; Szabova, L.; Sodeyama, K.; Iinuma, H.; Morita, R.; Gotoh, K.; Tateyama, Y.; Okubo, M.; Yamada, A. Sodium-Ion Intercalation Mechanism in MXene Nanosheets. *ACS Nano* **2016**, *10*, 3334–3341. [CrossRef]

Disclaimer/Publisher's Note: The statements, opinions and data contained in all publications are solely those of the individual author(s) and contributor(s) and not of MDPI and/or the editor(s). MDPI and/or the editor(s) disclaim responsibility for any injury to people or property resulting from any ideas, methods, instructions or products referred to in the content.